International Journal of Power Electronics and Drive System (IJPEDS)
Vol. 17, No. 1, March 2026, pp. 123~140
ISSN: 2088-8694, DOI: 10.11591/ijpeds.v17.i1.pp123-140

Impact and reliability analysis of voltage sags in a multi-pulse transformer-fed variable frequency drive system

R. Govarthanan[1,2], K. Palanisamy[1], S. Paramasivam[2]
[1]Department of Energy and Power Electronics, School of Electrical Engineering, Vellore Institute of Technology, Vellore, India
[2]Esab India Limited, Chennai, India

Article Info

Article history:

Received Jan 22, 2025
Revised Dec 22, 2025
Accepted Jan 23, 2026

Keywords:

FIDES
Multi-pulse transformer
Reliability
Variable frequency drive
Voltage sags

ABSTRACT

In an industrial grid, variable frequency drives (VFDs) are the major appliances that contribute to harmonic pollution. To reduce the effects of this harmonic pollution and comply with the regulatory standards, multi-pulse transformers are used to cancel out the specific harmonics. The VFDs experience a different input current profile when fed through multi-pulse transformers compared to direct grid connection. Despite the harmonic pollution reduction in the grid due to this implementation, the current stresses faced by the front-end devices will become higher. If the VFDs are designed only considering the impact of the direct grid consideration, the lifetime and reliability of the front-end devices will be a concern if operated with a multi-pulse feeder. This condition will be worse if there are presence of different types of sag events. This research details the effects of the reflected sags in the multi-pulse transformer's secondary windings and the current stresses in the different front-end converter elements due to this. Also, a systematic methodology using the FIDES approach is used to estimate the reliability of the front-end converter. A 7.5 kW-rated VFD is fed with a 12-pulse transformer is used for this research.

Corresponding Author:

K. Palanisamy
Department of Energy and Power Electronics, School of Electrical Engineering
Vellore Institute of Technology
Vellore 632014, India
Email: kpalanisamy@vit.ac.in

1. INTRODUCTION

A variety of power quality issues exist today, including harmonic distortion, frequency variation, noise, transient voltage spikes, outages, and sags. Power quality problems in VFDs have been documented in numerous research surveys and papers [1]-[3]. These studies indicate that voltage sags and long-term voltage unbalances are more severe than other power quality issues. Multi-pulse drives offer a simple, low-loss solution for meeting harmonic standards and provide flexibility to achieve limits with six-pulse diode bridges [4], [5]. Typically, voltage unbalances induce lower-order harmonic voltage components onto the DC bus voltage, increasing electrical stresses on the DC-bus choke inductor and the DC-link electrolytic capacitors. This shortens the capacitor's lifetime and increases inductor losses. Voltage unbalances increase the DC link ripple more than balanced voltage conditions, which inadvertently affects the torque ripple at the variable frequency drives (VFD) output, leading to increased induction motor heating and mechanical stress.

This paper focuses on twelve-pulse VFDs that contain two rectifier sections. The inputs of each rectifier section are connected to one of the secondary windings of the twelve-pulse transformer. The DC sides of these rectifiers are connected in parallel without an interphase reactor, serving as the input to the inverter, as shown in Figure 1. However, the rectifiers have DC link inductors to meet harmonic regulations and reduce

DC ripple in the capacitors [6], [7]. The DC link capacitors provide ride-through energy storage capacity and a low-impedance path for ripple currents.

Generally, DC link inductors and capacitors are designed to absorb 300 Hz harmonic voltage components when input voltages are balanced in six-pulse rectifiers [8], [9]. In twelve-pulse rectifiers, the capacitors must absorb 600 Hz components. In cases of voltage unbalances, low-frequency components (100 Hz, 200 Hz) will be present in the DC link voltage in both six-pulse and twelve-pulse cases. This increases capacitor losses and heat due to the low-frequency ripple current, reducing the capacitors' lifetime. Additionally, significant AC flux stresses the magnetic core material due to low-frequency harmonic voltage components. These components increase core losses in the inductor or lead to magnetic saturation, resulting in significant drops in effective inductance. Cumulatively, magnetic saturation increases SCR/diode current stresses, causing premature failures. In normal VFDs, extreme voltage unbalances are sensed by measuring DC link voltage ripples, but this method is ineffective for twelve-pulse connections. This research aims to clarify these issues and recommend alternative sensing approaches to designers.

The lifetime of capacitors is generally based on temperature, operating voltage, ripple currents, and ripple frequencies. Capacitor losses vary due to different operating conditions of the inverter and rectifier. Capacitor losses and heating effects in six-pulse rectifiers due to unbalances and phase loss conditions are described in earlier research [9], [10]. These studies also discuss capacitor ripple current variation due to pulse width modulation (PWM) operation of the inverter. Prolonged voltage sags often generate voltage unbalances, except for type A sags. Voltage unbalance conditions produced by different types of sags transform differently depending on the transformer type. In twelve-pulse cases, two different transformations occur based on the construction of the primary and secondary windings. This difference produces a considerable difference in the current stresses between the two rectifier components of the VFD. None of the earlier research has analyzed the voltage reflection in the secondary windings of the 12-pulse transformer during such sag scenarios and the effects on the rectifier components like DC Inductors and capacitors.

It is very important to know the behavior during such conditions, because most of the VFD manufacturers design the converter to work in a modular fashion for both six-pulse operation and twelve-pulse operation; however, they place more attention place more attention on the six-pulse condition as these are the higher-volume products. But, more attention needs to be given during the 12 pulse case w.r.t the DC link dynamics in case of sags and unbalance events, as the reliability of the front-end components will degrade considerably due to the presence of the sags and unbalances. This research considers a 7.5 kW 12 pulse VFD to verify the accuracy and effectiveness of the analysis by comparing the performance predictions of simulations and experimental results. The effect on the DC link inductor currents and the losses due to them is discussed, referring to [11]. The reliability of the capacitor has also been predicted based on the different mission profiles [12], [13] and through the FIDES methodology [14]. Some of the earlier research work [15]-[23] has been referred to for estimating the failure rate of the capacitor considering constant and wear-out failures. The impact of the grid imbalance for this case has been analyzed, referring to the research done in [24], [25].

2. TWELVE-PULSE VARIABLE FREQUENCY DRIVE SYSTEM

Twelve-pulse rectifiers have gained attraction in the present-day time, also as they meet the IEEE-519 requirements because of the simple topological advantage. Twelve-pulse rectifiers provide fewer losses and reduced control needs, as no active switching devices are involved. If the field installation has a twelve-pulse transformer facility, the overall cost of the twelve-pulse VFD system will be the same as that of the six-pulse VFD system, and it gets the advantage of meeting IEEE-519 needs. In a twelve-pulse variable frequency drive system shown in Figure 1, the input current will have harmonic components at 11, 13, 23, 25, 35, 37th multiples of fundamental frequency, wherein for a six-pulse variable frequency drive, in addition to this, 5, 7, 17, 19, 29, 31st multiples are also present. To achieve a twelve-pulse function in a variable frequency drive, most of the manufacturers use conventional six-pulse drives and connect the DC side of the rectifier portion in parallel, as shown in Figure 1. Ultimately, in the twelve-pulse drives, the DC link capacitors will experience reduced ripple currents compared to six-pulse drives. This is because the ripple voltage present in the DC link is less in magnitude, and the ripple frequency of the DC link voltage is 600 Hz, where the six-pulse drive will see 300 Hz. These factors will generally reduce the loss in the capacitors. But the diode/SCR bridges and the inductor will experience similar current conduction as that of the six-pulse rectifier case, with the phase shift in the currents. Because of this phenomenon, the stresses in the DC link components are not exactly the same as those of the six-pulse case. The use of interphase reactors can reduce this effect. But the design is more expensive, and many drive manufacturers do not prefer this option, and the modularity in the design will be lost. None of the earlier research has analyzed the stresses in the DC link components of twelve-pulse rectifiers in detail. The voltage reflected on the DC side of the VFD will be directly impacted by two parameters. The

first one is the voltage transformation in the secondary windings. The second one is the voltage variation in the transformation due to the voltage sags and their type. The following two sections describe the same.

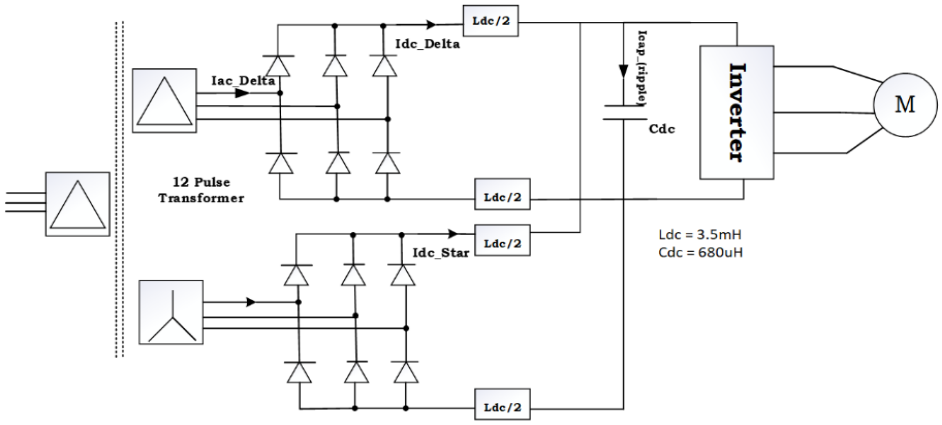

Figure 1. Twelve-pulse variable frequency drive

3. VOLTAGE TRANSFORMATION IN DIFFERENT TYPES OF TRANSFORMERS

The transformer types are classified into three categories. During the pre-fault voltages and during the fault conditions, the voltage transformation will be different with respect to different types of transformers in terms of magnitude and phase-angle. This is getting rotated without any influence on the equipment. Such phasor rotation can be seen as a shift in the zero point on the time axis, which, of course, has no influence on the equipment behavior. The three different types of transformers and their transformation are as explained below, referencing [3].

– Type 1: Transformers that do not change anything to the voltages. Here, the secondary voltages are equal to the primary voltages. This is possible with only a star-star (Yy) transformer with star points grounded. The following is the voltage transformation matrix of type1 transformer.

$$T_1 = \begin{bmatrix} 1 & 0 & 0 \\ 0 & 1 & 0 \\ 0 & 0 & 1 \end{bmatrix} \quad (1)$$

– Type 2: Transformer that can remove the zero-sequence component. The secondary voltages are equal to the voltages on the primary side, minus the zero-sequence voltage. The examples are Yy transformer with one or both points not grounded and a delta-delta (Dd) connected transformer. The following is the voltage transformation matrix of a type 2 transformer.

$$T_2 = \frac{1}{3}\begin{bmatrix} 2 & -1 & -1 \\ -1 & 2 & -1 \\ -1 & -1 & 2 \end{bmatrix} \quad (2)$$

– Type 3: Transformers that swap line and phase voltages. For these transformers, each secondary voltage equals the difference between two primary side voltages. The examples are delta-star (Dy) and the star-Delta (Yd) transformers. The following is the voltage transformation matrix of a type 3 transformer (3).

$$T_3 = \frac{j}{\sqrt{3}}\begin{bmatrix} 0 & 1 & -1 \\ -1 & 0 & 1 \\ 1 & -1 & 0 \end{bmatrix} \quad (3)$$

The previous discussions on the transformer voltage transformations are very important to consider, as it is directly linked with the twelve-pulse transformers. The twelve-pulse transformers will have the two secondary windings where one is delta-connected, and the other one is star-connected. The primary winding can be either a star or a delta connection. So, the voltage transformation in the secondary windings can be any one of the three transformation models as shown in (1), (2), and (3) based on the transformer arrangement.

4. TYPE OF VOLTAGE SAGS

The voltage sags are classified as type A to type D sags, as shown in the Table. 1. Type A sag is the balanced sag, and other sags are unbalanced sags. Type B sag is magnitude unbalanced sag, where type C and type D changes both magnitude and phase angle.

$$Unbalance\ [\%] = \frac{[V_{avg} - V_{\emptyset}]}{V_{avg}} \quad (4)$$

$$V_{avg} = \frac{V_a + V_b + V_c}{3} \quad (5)$$

Where V_{avg} is the average value of the three-phase voltages. $V_{\emptyset}$ is the individual phase voltage. Figure 2 shows the phasor diagram of three-phase voltages under such sag scenarios. These sags reflect balanced and unbalanced conditions according to their characteristics. The amount of unbalance is expressed according to IEEE is given in (4), where V_{avg} is shown in (5). Table 1 presents the phase voltage equations for different types of sags, where h is the sag depth in p.u. $V=V_L/\sqrt{3}$ phase to ground voltage.

These sags will be mainly generated due to single-phase faults and line-to-line faults, as three-phase faults are not common in many of the scenarios. The characteristic equations of these sags are given in equations in Table 1. The voltage phasors create an unbalanced situation in most of the sag conditions, except for type A sag. The type C and type D sags produce phase unbalances, along with magnitude unbalances.

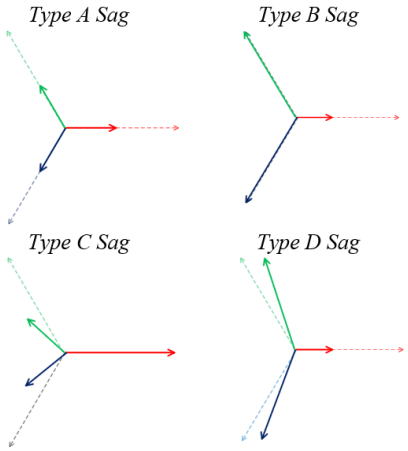

Figure 2. Four types of sags in phasor diagrams obtained [3]

Table 1. Four types of sags in equations obtained [3]

Parameters	Values
Type A Sag	$V_a = hV$
	$V_b = -\frac{1}{2}hV - \frac{1}{2}jhV\sqrt{3}$
	$V_c = -\frac{1}{2}hV + \frac{1}{2}jhV\sqrt{3}$
Type B Sag	$V_a = hV$
	$V_b = -\frac{1}{2}V - \frac{1}{2}jV\sqrt{3}$
	$V_c = -\frac{1}{2} + \frac{1}{2}j\sqrt{3}$
Type C Sag	$V_a = V$
	$V_b = -\frac{1}{2}V - \frac{1}{2}jhV\sqrt{3}$
	$V_c = -\frac{1}{2}V + \frac{1}{2}jhV\sqrt{3}$
Type D Sag	$V_a = hV$
	$V_b = -\frac{1}{2}hV - \frac{1}{2}jV\sqrt{3}$
	$V_c = -\frac{1}{2}hV + \frac{1}{2}jV\sqrt{3}$

5. SAG PROPAGATION IN TWELVE-PULSE TRANSFORMER

5.1. Twelve-pulse transformer configurations

Twelve-pulse transformer consists of two secondary windings and one primary winding. The secondary windings used to have star and delta connections. During the balanced voltage at the primary, the phase shift between these two secondary windings will be 30° based on the configuration to eliminate 5th and 7th harmonics in the rectifier. So, in a twelve-pulse transformer's primary current, 11th and 13th order harmonics will be the major. The currents shared by two secondary windings will be equal during balanced voltage and balanced load conditions. In the case of twelve-pulse three-phase rectifiers, as shown in Figure 1, and the secondary loads are balanced, the currents or current harmonics carried by the individual rectifier will be balanced until the balanced voltage is present in the primary transformer. Few earlier researchers have addressed the analysis of twelve-pulse transformer functionality [4], [5] and briefly explained this. A twelve-pulse transformer with a delta primary winding is considered for this analysis. Additionally, for simplicity, instead of considering one single three-winding transformer, two two-winding transformers are considered. The vector group of these two transformers is Dy1 (delta-star) and Dd0 (delta-delta).

5.2. Sag propagation in a twelve-pulse transformer

During the normal balanced operating conditions of a twelve-pulse transformer, the transformation of voltages from primary to secondary windings is described in earlier sections. But during the sag scenario, the phase and amplitude will vary between the secondary windings because of the transformer configurations and different sag transformation phenomena. Considering the twelve-pulse transformer configuration as per Figure 1, the transformation of sag type in the secondary side, as shown in Table 2, referring to [1].

So, the expected voltage and current variations in the secondary windings will be different in the case of the twelve-pulse rectifiers during sag and unbalanced conditions. For example, in the case of a type B sag scenario, the reflected effect at the secondary winding's delta and star of the transformer will be type D and type C, respectively. This creates different phase and magnitude deflection between the two secondary windings compared to the balanced operating condition. This creates a different scenario in rectifier conduction as well. This scenario will create an unbalanced current conduction in between the rectifiers and the DC link inductors. This will lead to the creation of high ripple currents in the DC link capacitors due to the presence of low-frequency components other than 300 Hz. The next section will analyze this phenomenon in detail through simulation and experimental results. The paper will focus on the impact of type A and type B sags in the primary side of a twelve-pulse rectifier system and the reliability of different devices. The resultant effects expected are like the scenarios of type C and type D, as mentioned in Table 2. In the further sections, only the effect of sags and unbalances produced by type A and type B sags will be discussed because of this.

Table 2. Transformation of sag type to secondary windings vs various primary sags

Prim side sag (delta)	Type A	Type B	Type C	Type D
Reflected sec. Side sag (delta)	Type A	Type D	Type C	Type D
Reflected sec. Side sag (star)	Type A	Type C	Type D	Type C

6. EFFECTS OF SAGS IN RECTIFIER COMPONENTS

A 7.5 kW, 500 V, twelve-pulse VFD setup is used to evaluate the drive characteristics with DC link inductor characteristics. Figure 3(a). shows the experimental and measurement setup with an induction motor load setup, and the measured results are presented in Figure 3(b). Figure 3(c) confirms very good agreement with the simulated results with the balanced input voltage. The twelve-pulse transformer has primary star configuration has been considered for the analysis. The simulation and practical experiments have been extended with different sag scenarios according to Table 2 to analyze the effect of the sags on the twelve-pulse VFD sections in the next sections.

6.1. Type A sag and the effect

Type A sag is a voltage-balanced sag. The increased sag depth produces the balanced sag reflection in both the secondary sides of the transformers. Because of this fact, during any sag, the rectifiers will be stressed equally. Figure 4 shows the simulation results at type A sag scenario.

6.2. Type B sag and the effect

Type B sag is an unbalanced sag with respect to the magnitude. But when the type B sag is applied at the primary winding of the twelve-pulse transformer, it reflects into type C and type D sag in star and delta winding, respectively.

Figure 5 is the simulation result of the sag reflection at the twelve-pulse secondary windings when type B sag with the sag depth of 0.9 is applied at the primary. Figures 6(a) and 6(b) are the practical results of the reflected waveforms at the delta and secondary voltages, respectively. The measurement proves that the type-B sag in the primary is reflected as type D sag in the Delta secondary winding and type C sag in the star secondary winding. The results in Figures 6(a) and 6(b) confirm the sag reflection in Table 2. The simulations and experiments were extended type B sag scenario applied at the primary side of the twelve-pulse transformer with varying per unit sag depths from 0.1 to 0.7. The results are shown in Figure 7. The results show the variation in the currents between two secondary windings along with the variation of different sag depths. In general, the sag depth can vary between 10% to 90% according to the definition given in IEEE 1159–1995. The effect of various rectifier components has been presented based on the simulation results. Figures 7 and 8 show the simulation results of different sag conditions and their effect on the rectifier current and inductor currents. It is noted that the reflected currents at the secondary windings of the twelve-pulse transformer are different from winding to winding during the type B sag scenario compared to the type A sag. This is because of the sag transformation between the primary and secondary windings during type B sag, as shown in Table 2.

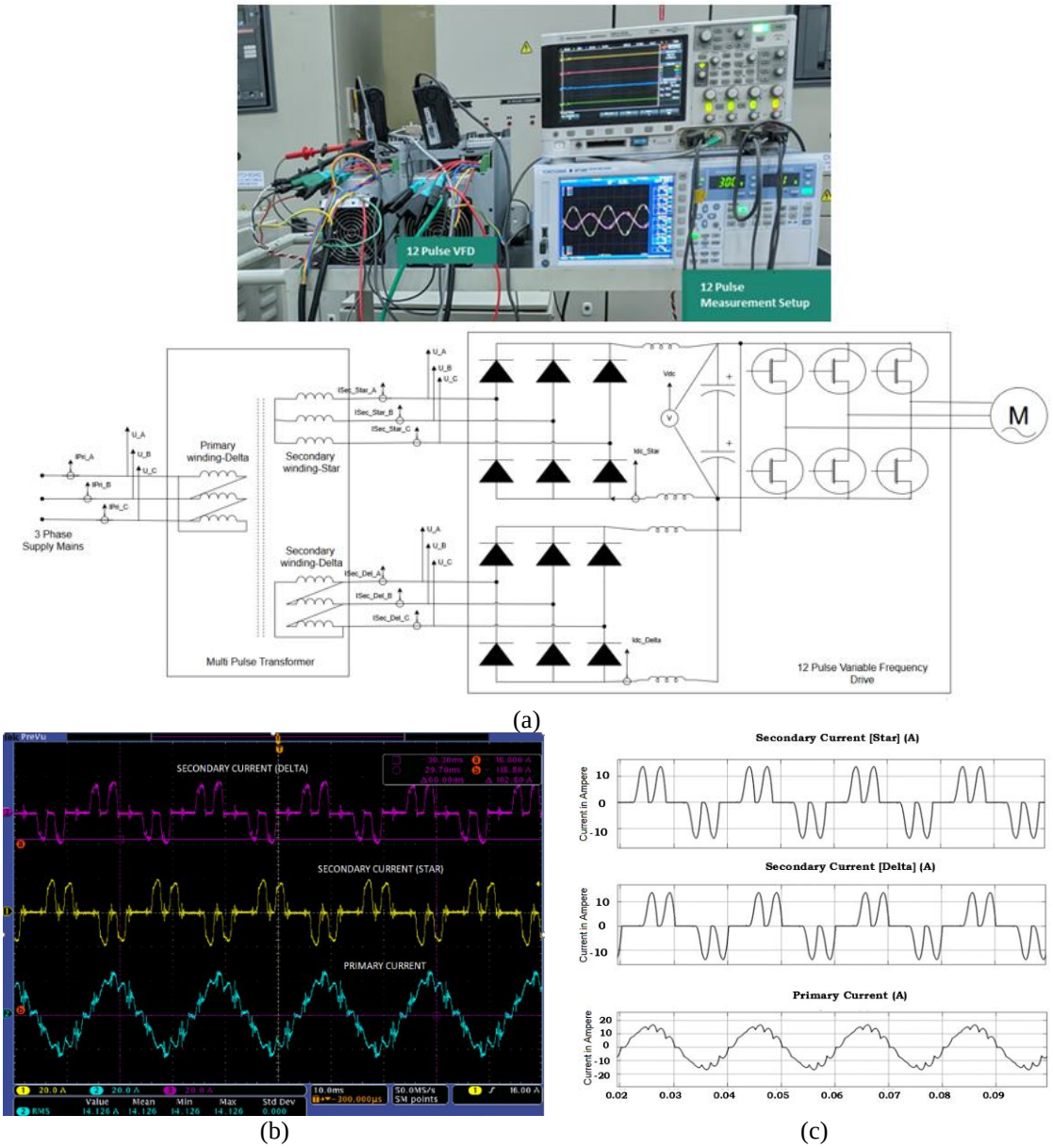

Figure 3. Verification of sag scenario with simulation and practical results at balanced conditions: (a) 7.5 kw twelve pulse VFD experimental and measurement setup, (b) practical test results twelve-pulse rectifier system, and (c) simulation results of the twelve-pulse rectifier system

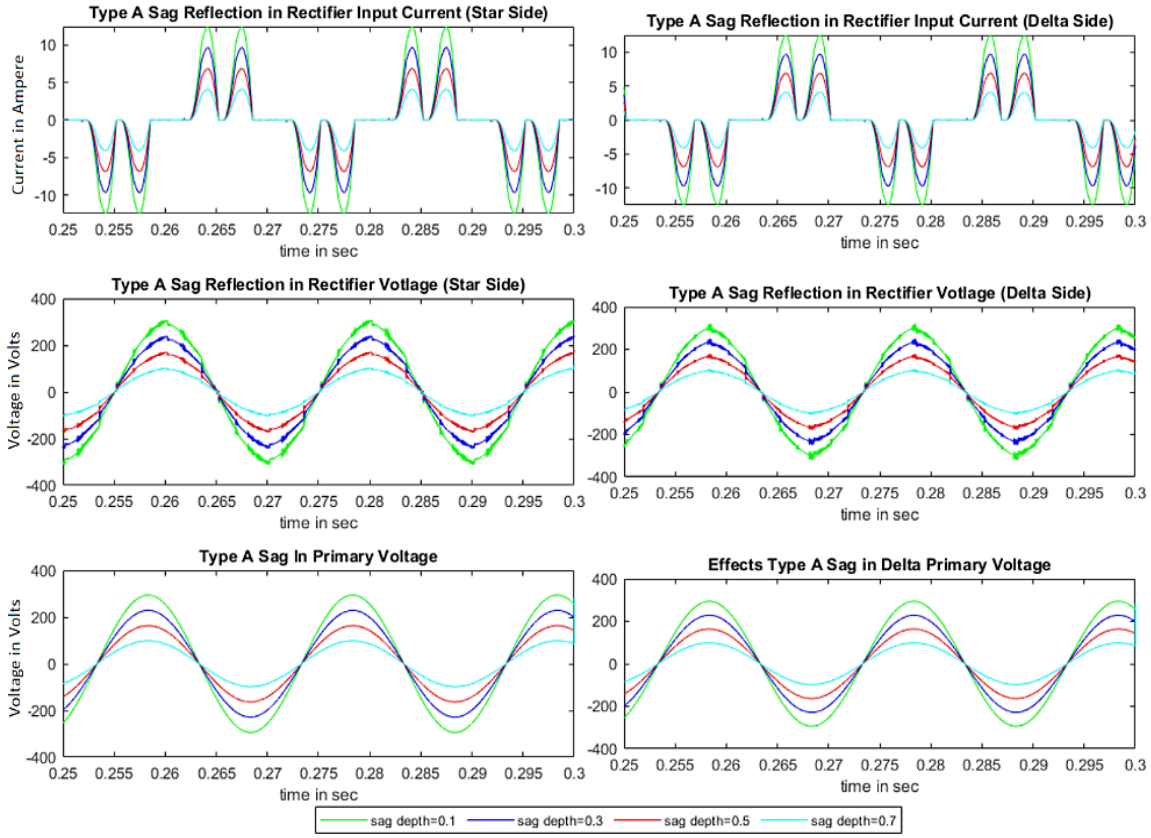

Figure 4. The measured rectifier parameters for varying type A sag depth from 0.1 to 0.7

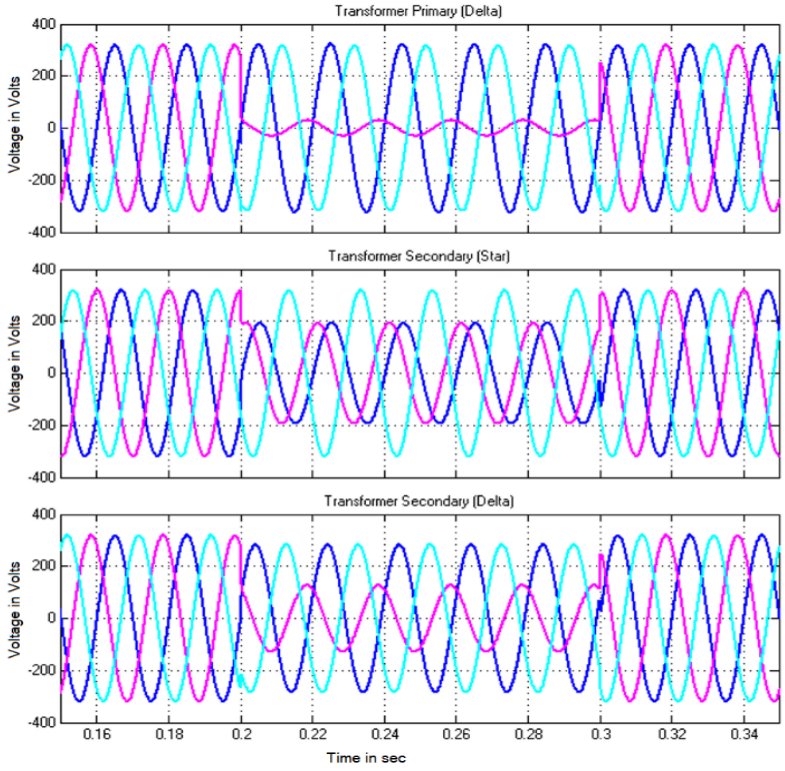

Figure 5. Type B sag transformation in the secondary windings (simulation results at sag depth = 0.9)

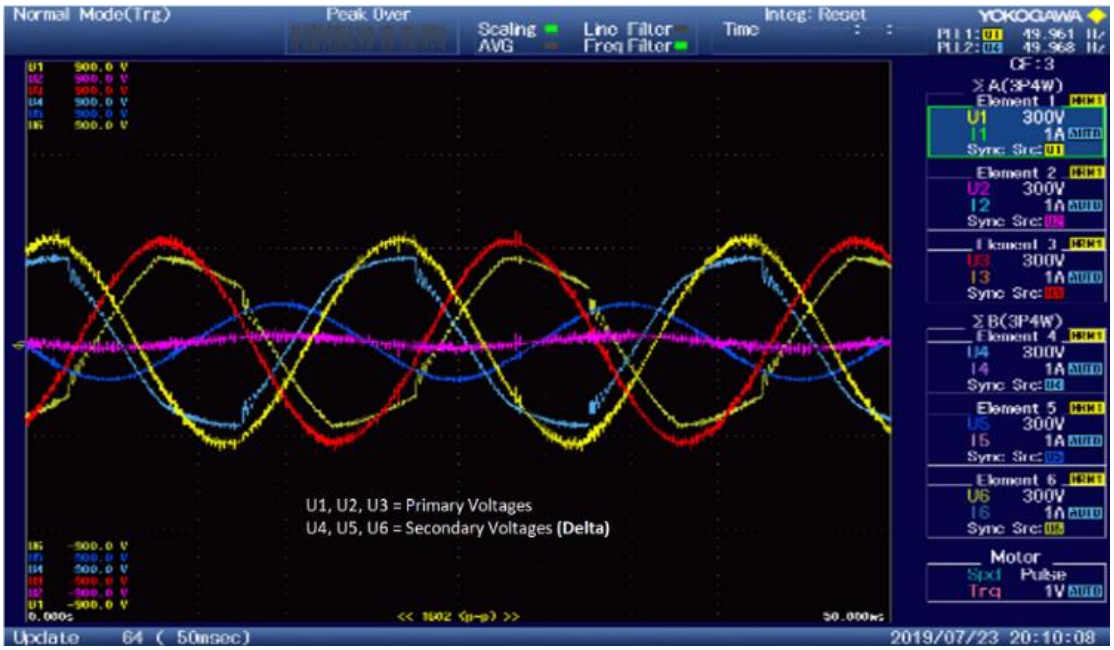

(a)

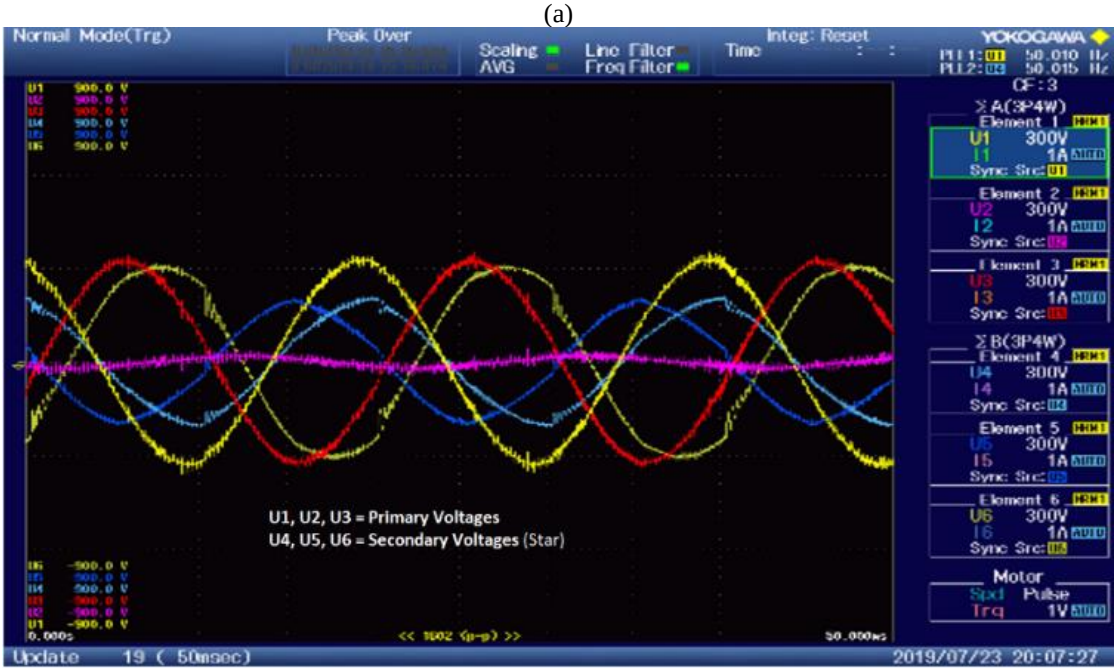

(b)

Figure 6. Practical validation of sag reflections: (a) type B sag at sag depth = 0.9 at delta side and (b) type B sag at sag depth = 0.9. at star side

Seeing the results, the unpredicted effects will be one of the rectifier sides will be very serious in case of type B sag and its depth. The further sections of this paper will focus on the stresses and reliability of the rectifier components due to type B sag during the possible sag conditions. Type B sag is an unbalanced sag, So the effect of this sag will be analyzed in terms of amount of unbalance in the primary voltage. In general, the VFD shall be aimed to work under 3% Unbalance condition and phase loss conditions, where the VFD must perform with or without the power limitations during these conditions. So, the analysis has been extended to see the effect on the DC link inductor and capacitor stresses in in 3% voltage unbalance and phase loss situation. The current imbalances will impact on the multi-pulse transformer losses and its reliability as well. However, in this research this has not been dealt with in detail. Because in many cases, the drive will be fed from a common multi-pulse transformer which supplies multiple drives, where the impact on the transformer is less compared to the drive components.

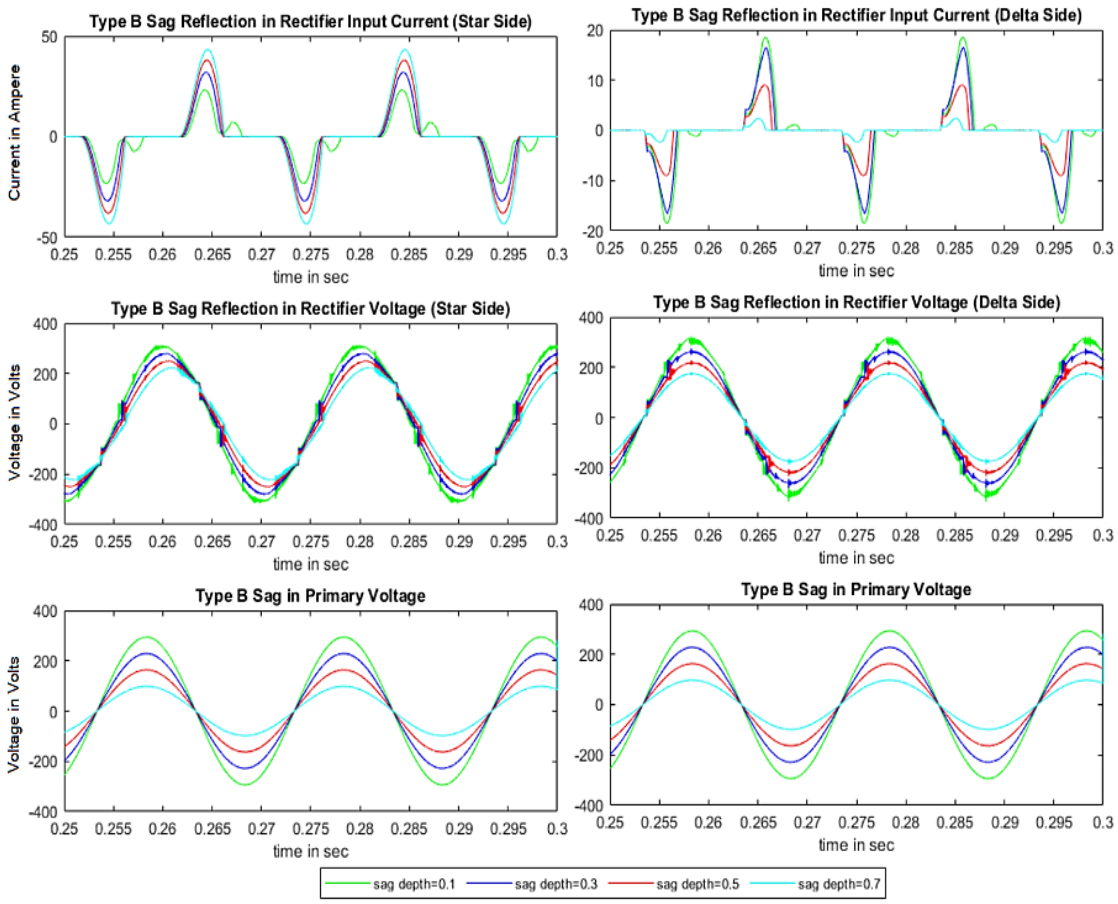

Figure 7. The measured rectifier parameters for varying type B sag depth from 0.1 to 0.7

7. DC LINK INDUCTOR STRESS EVALUATION

The advantages of DC link inductors during balanced and unbalanced conditions of input voltage supply have been summarized in the introduction. During the unbalanced condition, the effect of 100 Hz component will be very high in the DC link, which leads to increased DC current peaks. This current peak may lead to DC inductor saturation. If the VFD does not have the prediction of such scenario by measuring the DC link voltage, the reflected harmonics and peak current will be increased at the input side due to the inductor saturation. But the presence of 100 Hz component creates a high AC voltage across it in case of six-pulse cases. This condition will be different in the case of twelve-pulse operation under the influence of different types of sags. A 7.5 kW twelve-pulse VFD system operating at different depths of sags under type A and type B scenarios at the primary, and the DC link inductor develops an AC voltage which contains both 100 Hz and 300 Hz components. This has been shown in Figure 8. The current waveform is considerably different between the two DC limb inductors. As the effect of type A sag does not create a difference between the secondary input currents as shown in Figure 6, the effect of type B sag is only presented below. The simulation has been further extended for operating in phase loss or single phasing condition (considering type B sag depth of greater than 0.9) and different voltage unbalance conditions to check the effects in the inductor current harmonics and capacitor current harmonics for further analysis. This analysis is intended to understand and identify the VFD's critical operating conditions which leads to failure or degradation of lifetime. From the results, it is shown that the DC link inductor stressed variably between the two secondary rectifiers during the time of sag. From the results of the measurements, the deviation in the inductor currents in between the two secondary windings are shown in Figure 9.

7.1. Losses in the DC inductor

The DC link inductor serves to reduce the input current harmonics; additionally, it protects the inverter from input current surges. The DC link inductor is usually designed for handling 300 Hz components as many manufacturers consider the cost attractiveness and for getting compact design. The critical operating conditions due to phase-loss and unbalance conditions are not being given in-depth attention during the design of DC

Inductor. During the unbalanced and phase-loss condition, the DC link inductor experiences huge voltage fluctuations across it, as shown in Figure 8. The inductor voltage drop contains various frequency components apart from 300 Hz. This is a natural phenomenon in a six-pulse drive, also. But considering the reflection of type B sag in the twelve-pulse drives, the effect gets aggravated. The influence of the 100 Hz component is considerably strong during this time. The harmonic multiples of 100 Hz and 300 Hz components are also present. The difference in this effect is high in between the two inductors of two rectifier circuits in case of twelve-pulse.

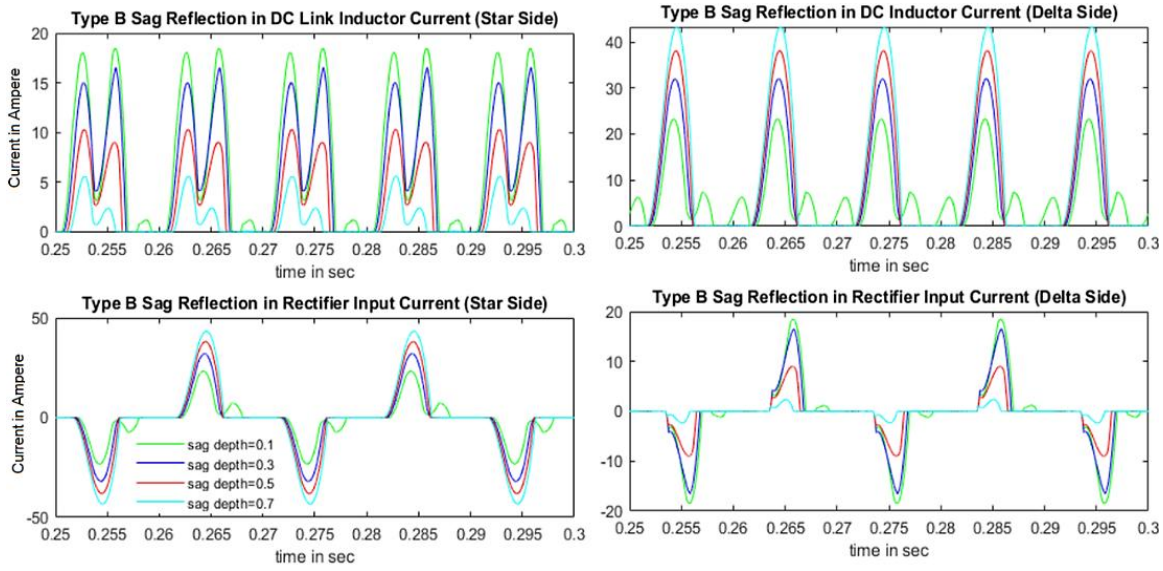

Figure 8. DC inductor current stress with respect to input current variation during type B sag

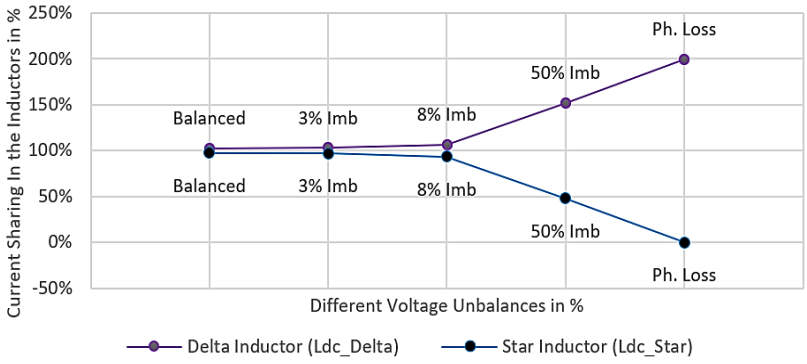

Figure 9. Percentage deviation in the current sharing between the star side and delta side inductor

The governing equations for flux density estimation [8] are given in (6), (7), and (8).

$$B_{ac_h} = \frac{E_h \, x \, 10^4}{K_f \, . \, f_h \, . \, A_c \, . N} \tag{6}$$

$$B_{dc} = \frac{(0.4).\pi.N.I_{dc}.\mu.(10^{-4})}{MPL} \tag{7}$$

$$B_{pk} = B_{dc} + \sum_{h=1}^{\infty} B_{ac_h} \tag{8}$$

Where B_{dc} is the DC flux density, Bac is the AC flux density contributed by different harmonic components, N is the number of turns in the inductor, f_h is the harmonic frequency, A^c is the core area, E_h is the amplitude

of hth order component, MPL is the magnetic path length, h is the order of harmonic, μ is the permeability of the core. The peak flux density (B_{pk}) is determined by (8). The B_{pk} varies based on the individual harmonic contribution. Figures 10(a) and 10(b) show the harmonic spectrum of the DC inductors during three different operation conditions. Figures 11(a) and 11(b) show the inductor current waveforms during phase-loss and 3% unbalanced condition, respectively. From these figures, it is clearly understandable that the entire inductor profile between the two secondary sides is totally different. The volt-sec product of the inductor is proportional to the flux linkage or change in the current of the inductor.

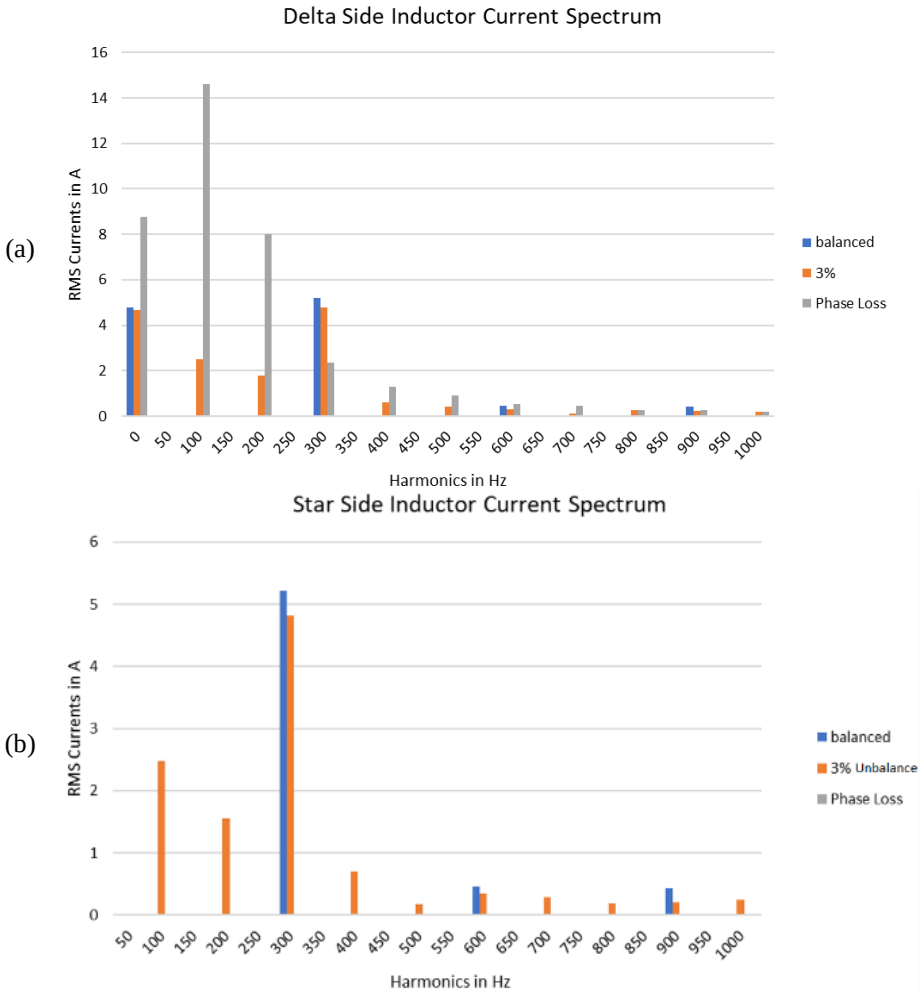

Figure 10. DC inductor harmonic variations: (a) star side during type B sag in primary side and (b) delta side during type B sag in primary side

So, there will be a considerable difference in the volt-sec product when the inductors are subjected to unbalanced condition and phase loss condition. It is hard to say that the additional harmonic components in the magnetic flux linkage will affect the inductor to enter in saturation of the magnetics without having the specification of the inductor parameters and design. But during balanced operations, the majority will be the 300 Hz component in both star side and delta side inductors and Balanced. But during phase-loss conditions, the 100 Hz component is considerably high only in the Delta side inductor and negligible in star side inductor. This creates considerable current variation between these two inductors which in turn varies the loss distribution as well. From Figure 10, it is shown that the harmonic current spectrum variation in between the secondary windings is considerable when there is a type B sag of more than 0.9 depth (phase-loss condition).

The difference in 100 Hz component is considerably high during this condition. For analysis purpose, a commercially available powder core inductor [11] is taken which has the core loss density characteristics is shown in Figure 12. for two different critical frequencies. The detailed inductor design for this purpose is not explained here. However, the loss density estimation is done for the inductor [8]. But the parametric

comparison of this core with different flux densities and the core loss variation is shown here. The formulae for core loss density for this core is given in (9).

$$P_L = 136.93.B^{1.781}.f^{1.12}\ mW/cm^3 \quad (9)$$

Estimation of core loss density is done for the DC link inductor for these three conditions are shown in Table 3. From Table 3, it is understandable that the losses due to the 100 Hz component is considerably high in case of phase-loss and unbalanced operating conditions, particularly in the delta side inductor. The losses are not distributed evenly between the two inductors because of the higher sag depth. These losses will be further aggravated by the local heating of the inductor. The deviation in the currents as shown in Figure 9 cannot be estimated unless there is a measurement in the input current of individual rectifiers or inductor current measurements. If the unbalance condition or the phase-loss conditions persists for long time, the additional losses will increase the inductor temperature significantly to the dangerous levels if these harmonics are not considered adequately while designing the DC link inductor. Note that in this research only core losses are considered as the deviation in the copper losses between inductor are small during these conditions.

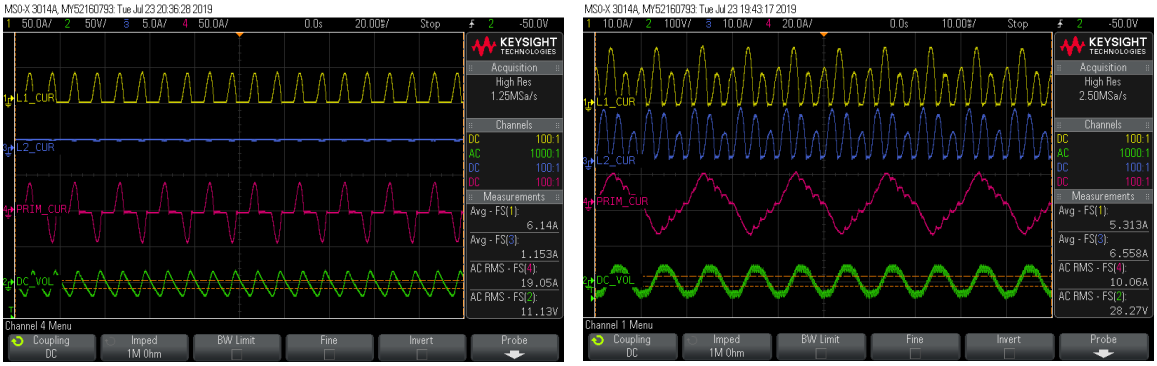

(a) (b)

Figure 11. Measurement results during different sag scenarios: (a) phase loss condition [yellow: delta side DC inductor; blue: star side DC inductor, pink: primary current, green: DC ripple voltage] and (b) 3% imbalance condition [yellow: delta side DC inductor; blue: star side DC inductor, pink: primary current, green: DC ripple voltage]

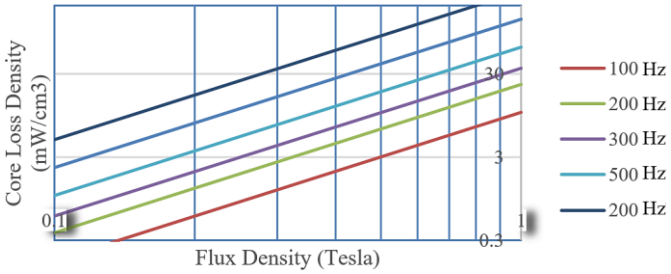

Figure 12. Core loss characteristics of commercial core 0077083A7 from magnetics.inc®

Table 3. Core loss distribution between two DC inductors due to different harmonic influences

Secondary Winding Configuration	Harmonic		Balance	3% Imb	8% Imb	50% Imb	Ph.* Loss
Star secondary winding	100 Hz	[W]	0.0001	0.364	0.901	0.448	0
	300 Hz	[W]	3.309	2.914	2.249	0.87	0
	600 Hz	[W]	0.113	0.215	0.337	0.158	0
	900 Hz	[W]	0.429	0.183	0.175	0.059	0
	Total	[W]	3.803	4.9	5.2	2.98	0
Delta secondary winding	100 Hz	[W]	0.0001	0.366	1.053	2.567	3.531
	300 Hz	[W]	3.229	2.899	1.927	1.395	1.157
	600 Hz	[W]	0.314	0.180	0.095	0.306	0.364
	900 Hz	[W]	0.453	0.182	0.117	0.157	0.253
	Total	[W]	3.997	5.229	5.93	9.505	11.16

* As there is no conduction in the star rectifier during the phase loss condition, no watt-loss is present

8. ESTIMATION OF LOSSES AND LIFETIME IN DC CAPACITORS

Many factors affect the lifetime of the electrolytic capacitors in VFDs. These can be the voltage applied, ripple current, operating temperature, air flow, as well as the equivalent series resistance (ESR) of the capacitor. The increase in the operating DC link voltage will increase the additional leakage current, which will increase electrochemical degradation and hydrogen gas evolution. This will, in turn, reduce the lifetime of the capacitor. Different manufacturers refer to different approaches to estimate the lifetime of the capacitors. The following steps are taken for estimating the lifetime of the capacitors [9]. The ripple presence at the DC link in a twelve-pulse rectifier is different from the six-pulse case. Most of the components are due to 600 Hz in the case of twelve-pulse, where it is 300 Hz in six-pulse rectifiers.

8.1. Know the ripple current spectrum of the capacitor

The lower-order ripple currents (100 Hz, 200 Hz, 300 Hz, and 600 Hz) used to be considered considerable for calculating losses. As the ESR used to be high at the lower order harmonics. The higher-order harmonics should also be determined for calculation.

8.2. Understand the ESR profile of the capacitor

The ESR is the frequency-dependent parameter as shown in Figure 13. The ESR profile will be based on the manufacturer and the type of electrolytic capacitor [13], [20], [21]. The capacitor ESR model is shown in (10).

$$Z_{cap} = \frac{1}{\frac{1}{R_2 + j2\pi f C_2}} + R_I + R_0 - \frac{j}{2\pi f C_1} \quad (10)$$

Where Zcap: complex impedance of capacitor, R0: foil and terminal resistance, R1: resistance of electrolyte, R2: dielectric loss resistance, C1: terminal capacitance (F), and C2: dielectric loss capacitance (F).

$$ESR = Real\ (Z_{cap}) \quad (11)$$

$$Real(Z_{cap}) = \frac{R_2}{1+(2\pi f)^2 {C_2}^2 {R_2}^2} + R_1 + R_0 \quad (12)$$

The equivalent ESR will be calculated based on the individual harmonic magnitude of the capacitor ripple current. At very high frequencies beyond 2 kHz, ESR will be constant as R2 will be bypassed by the capacitance C2.

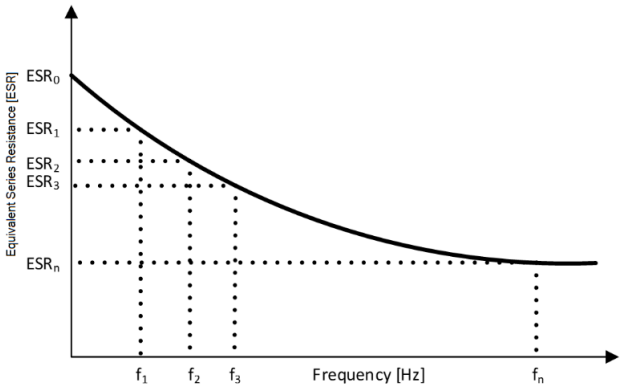

Figure 13. ESR variation (vs) different harmonic frequencies

8.3. Calculate the increase in temperature ΔTx

The increase in temperature can be calculated using (13). The increase in temperature needs to be found out for each harmonic component identified by knowing the ESR and I_{rms} value in each harmonic content.

$$\Delta T_x = R_{th} \,.\, ESR \,.\, {I_{rms}}^2 \quad (13)$$

8.4. Calculate the lifetime of the capacitor

The lifetime L_t can be calculated [1] using (14). Where T_o and T_x are rated and actual ambient temperatures, respectively.

$$L_t = L_{t_o}.\left[2^{(T_o-\frac{T_x)}{10}}\right].\left[2^{\frac{T_o-T_x}{k}}\right].\left[\frac{V_o}{V_x}\right]^{4.4} \quad (14)$$

V_o and V_x are the rated and actual applied voltage, respectively. L_{to} is the load life rating provided by the manufacturer. k is the acceleration factor, which varies based on the temperature ΔT_x and the order of the harmonic content, which will be supplied by the capacitor manufacturer. The values of capacitor RMS currents predicted lifetime are captured in Table 4 for a commercially available capacitor of CGS681T450R4C [22]. There are four capacitors, where one set has two capacitors connected in series and two sets are connected in parallel to get an equivalent of 680 uF in the DC link.

Table 4. Lifetime estimation of DC capacitors on different sag and unbalanced conditions

Mission profile	Operating condition	Ripple current [A]	Power loss [W]	Temperature rise [degC]	Life time [Hrs]
Mission profile - 1	Balanced	1.174	0.124	4.9	66313
Mission profile - 2	3% Imbalance	5.469	2.692	10.63	49288
Mission profile - 3	8% Imbalance	6.745	4.094	16.17	41917
Mission profile - 4	50% Imbalance	7.985	5.738	22.67	34665
Mission profile - 5	Phase Loss	10.241	9.44	37.3	22603

From the measurement and calculation results, the ripple currents progressively increase w.r.t the amount of variation in sag depth. The ripple current variation is used to be estimated by the VFDs by measuring the DC link voltage ripple. In twelve-pulse drives, the ripple current variation can be precisely estimated only if there is a clear understanding of the response during different sag depths. The above results are helpful for the designers while estimating the lifetime of the capacitor, considering the abnormal conditions and the allowable time for operating the rectifiers. From the above analysis, it is evident that the design can be improved by reducing the ripple current of the capacitance. One of the methods to increase the lifetime is to increase the value of capacitance and inductance in the DC link to reduce the ripple current. This will ultimately improve the lifetime of these components.

9. THE FIDES BASED FAILURE RATE OF THE POWER CONVERTER

The most vulnerable component within the front-end rectifier system is the capacitor, which is prone to wear-out failures compared to the inductor and the rectifier diodes. So, in this paper, the capacitor failure rate is discussed, considering that the converter's failure rate is determined based on the capacitor. For estimating the probability of the failure rate, the five different mission profiles are shown in Table 4. By considering the different Imbalance levels. The failure rate is estimated based on the FIDES approach [16], where it has two different components: constant failure rate and non-constant failure rate. Constant failure rate is estimated from any generic guidelines [7] or the data source available with the component manufacturer. The generic failure rate data for different electronic components are provided in the MIL-HDBK-217F standard. This generalizes failure rates considering different operating conditions, including ambient temperature, operating current, and operating voltage. But obtaining reliability by considering a specific mission profile is not available in this approach. So, the FIDES approach gives the failure rate in time (FIT) prediction using the physics of failure and considering the mission profile. By using the FIDES approach, the failure rate (λ) is predicted using the following formulas.

$$\lambda = \Pi_{PM}\Pi_{Processes}\lambda_{phy} \quad (15)$$

$$\lambda_{phy} = \sum_{i=1}^{Phase}\left[\frac{t_{annual}}{8760}\right]_i \Pi_i\lambda_i \quad (16)$$

$$\Pi_i = \left(\Pi_{placement}\Pi_{app}\Pi_{rugg}\right)^{0.511.ln\,(Cs)} \quad (17)$$

$$\lambda_i = \sum_k \lambda_{0k}\Pi_k \quad (18)$$

In which, Π_{PM} impact of quality control and Π_{PM} effects on the process from specification to field operation and maintenance. λ_{phy} is the physical contribution model of the failure rate. λ_{phy} is calculated according to [16], which comprises the mission profile. λ_i is the failure rate during the i^{th} phase of the mission profiling, where it is calculated by knowing the base failure rate λ_{ok} and the acceleration factor $\Pi_{k,}$ which will reflect the physical constraints the item experiences during dormant phases.

The wear-out distribution of the components is estimated by stress-strength analysis. The applied mission profile is translated into the stress of the components. This intern will predict the probability of failure. The component strength is estimated by having a better understanding of the physics of the failures. The failure probability will be due to the stress of the component being higher than its strength. The wear-out failure distribution is explained in [15]. Here, the wear-out distribution of the electrolytic capacitor is estimated for the nominal operating conditions, where it is modeled with the Weibull distribution with α = 6804 hours and β = 5.12. For the specified mission profiles as in Table 4, the lifetime prediction is predicted by adjusting the base life distribution under nominal conditions as stated in [14]. From the analysis, the total failure rate is predicted in Figure 14. Figure 15 shows the constant failure rate and wear-out failure rate distribution.

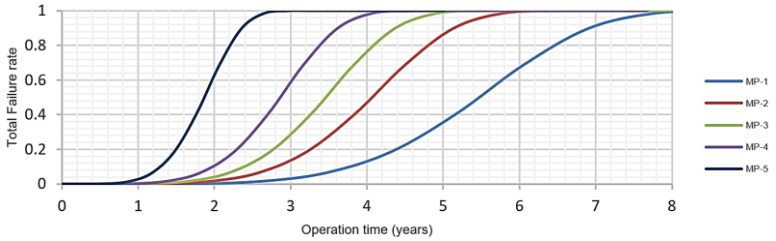

Figure 14. Total failure rate and reliability for the DC capacitor

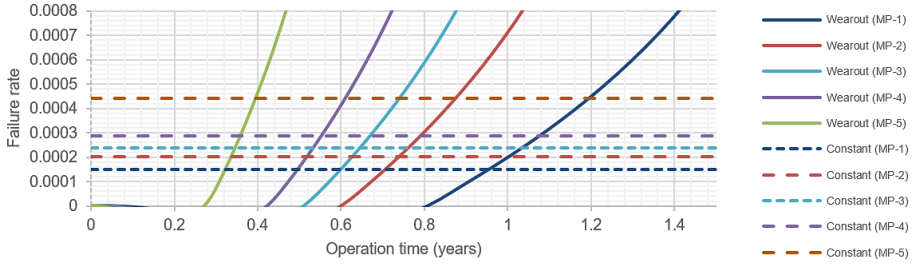

Figure 15. Distribution of constant and wear-out failure rate and reliability

10. CONCLUSION

This paper details the effect of various types of voltage sags and imbalances in the front-end converter of multi-pulse transformer-fed drives. Various types of sags and their reflection in the multi-pulse transformer secondary have been analyzed. A case study of a 7.5 kW VFD system with two rectifiers that has been fed by a 12-pulse transformer is presented. The current reflections in each rectifier section are simulated and tested during different sag types and depths. The mission profiles considering five different operating scenarios have arrived. The frequency spectrums for the capacitor ripple current and the inductor current were captured for these mission profiles. With this information, the loss calculations are performed for the inductors and DC capacitors, considering the five critical mission profiles. A lifetime model for the capacitor is created, and the expected lifetime for the different mission profiles has been calculated. From the results, it is shown that the lifetime with a sustained voltage unbalance of 3% deteriorates the lifetime by 30%. A reliability analysis was done for these mission profiles, considering the lifetime of the capacitor using the FIDES methodology. The estimation of MTBF and FIT curves are obtained. From this study, the expected failure rate with mission profile-5 (phase loss condition) will happen 1 year ahead of the mission profile-1 (balanced condition). As a conclusion, it is recommended that the estimation of the imbalance profiles is very important during the multi-pulse operation. Sizing the right value of input or DC reactors on the drive side can minimize the effect. Using interphase reactors between the rectifiers will be another option. The extension of this research can be done to estimate the value of inductance or interphase reactors for minimizing the effect and to estimate the lifetime of the capacitors with load frequency effects in the presence of different sag depths. Although the case study reveals the methodology to predict the reliability of a multi-pulse VFD, the same methodology can be used for other multi-pulse-fed rectifier applications.

ACKNOWLEDGEMENT

The authors like to express sincere gratitude to Danfoss Advanced Drives Laboratory, VIT University, for making this research work for execution and technical implementation in real time.

FUNDING INFORMATION

Authors state no funding involved.

AUTHOR CONTRIBUTIONS STATEMENT

This journal uses the Contributor Roles Taxonomy (CRediT) to recognize individual author contributions, reduce authorship disputes, and facilitate collaboration.

Name of Author	C	M	So	Va	Fo	I	R	D	O	E	Vi	Su	P	Fu
R. Govarthanan	✓	✓		✓	✓	✓		✓	✓	✓			✓	
K. Palanisamy		✓		✓	✓	✓		✓	✓	✓	✓	✓		
S. Paramasivam	✓						✓			✓	✓		✓	✓

C : **C**onceptualization
M : **M**ethodology
So : **So**ftware
Va : **Va**lidation
Fo : **Fo**rmal analysis
I : **I**nvestigation
R : **R**esources
D : **D**ata Curation
O : Writing - **O**riginal Draft
E : Writing - Review & **E**diting
Vi : **Vi**sualization
Su : **Su**pervision
P : **P**roject administration
Fu : **Fu**nding acquisition

CONFLICT OF INTEREST STATEMENT

Authors state no conflict of interest.

DATA AVAILABILITY

Derived data supporting the findings of this study are available from the corresponding author, [RG], on request.

REFERENCES

[1] K. Lee, T. M. Jahns, T. A. Lipo, G. Venkataramanan, and W. E. Berkopec, "Impact of input voltage sag and unbalance on DC link inductor and capacitor stress in adjustable speed drives," in *Fourtieth IAS Annual Meeting. Conference Record of the 2005 Industry Applications Conference, 2005.*, IEEE, pp. 1457–1463, doi: 10.1109/IAS.2005.1518551.

[2] Y. Wang, H. Yang, X. Xiao, and Y. Yang, "A low-data-dependence assessment method of industrial process interruption probability due to voltage sag," *IEEE Transactions on Power Delivery*, vol. 37, no. 6, pp. 5267–5277, 2022, doi: 10.1109/TPWRD.2022.3175162.

[3] M. H. J. Bollen, *Understanding Power Quality Problems*. New York, NY, USA: Willey-IEEE Press, 1999. doi: 10.1109/9780470546840.

[4] B. Singh, S. Gairola, B. N. Singh, A. Chandra, and K. Al-Haddad, "Multipulse AC-DC converters for improving power quality: A review," *IEEE Transactions on Power Electronics*, vol. 23, no. 1, pp. 260–281, 2008, doi: 10.1109/TPEL.2007.911880.

[5] D. A. Rendusara, A. von Jouanne, P. N. Enjeti, and D. A. Paice, "Design considerations for six pulse and twelve pulse diode rectifier systems operating under voltage unbalance and pre-existing voltage distortion with some corrective measures," in *IAS '95. Conference Record of the 1995 IEEE Industry Applications Conference Thirtieth IAS Annual Meeting*, IEEE, 1996, pp. 2549–2556, doi: 10.1109/IAS.1995.530627.

[6] P. N. Enjeti and P. D. Ziogas, "Analysis of a static power converter under unbalance: A novel approach," *IEEE Transactions on Industrial Electronics*, vol. 37, no. 1, pp. 91–93, 1990, doi: 10.1109/41.45849.

[7] D. A. Rendusara, A. Von Jouanne, and P. N. Enjeti, "Design considerations for 12-pulse diode rectifier systems operating under voltage unbalance and pre-existing voltage distortion with some corrective measures," *IEEE Transactions on Industry Applications*, vol. 32, no. 6, pp. 1293–1303, 1996, doi: 10.1109/28.556631.

[8] "IEEE recommended practice for electric power distribution for industrial plants." IEEE, Piscataway, NJ, USA, Dec. 02, 1993. doi: 10.1109/IEEESTD.1994.121642.

[9] K. Lee, T. M. Jahns, G. Venkataramanan, and W. E. Berkopec, "DC-bus electrolytic capacitor stress in adjustable-speed drives under input voltage unbalance and sag conditions," *IEEE Transactions on Industry Applications*, vol. 43, no. 2, pp. 495–504, 2007, doi: 10.1109/TIA.2006.889910.

[10] K. Lee, T. M. Jahns, W. E. Berkopec, and T. A. Lipo, "Closed-form analysis of adjustable-speed drive performance under input-voltage unbalance and sag conditions," *IEEE Transactions on Industry Applications*, vol. 42, no. 3, pp. 733–741, 2006, doi: 10.1109/TIA.2006.872953.

[11] Magnetics Inc., "Powder Cores." [Online]. Available: https://www.mag-inc.com/Products/Powder-Cores

[12] Z. J. Fang, T. Cai, S. X. Duan, C. Chen, and C. Da Ren, "Performance analysis and capacitor design of three-phase uncontrolled rectifier in slightly unbalanced grid," *IET Power Electronics*, vol. 8, no. 8, pp. 1429–1439, 2015, doi: 10.1049/iet-pel.2014.0421.

[13] D. Rendusara, E. Cengelci, P. Enjeti, and D. C. Lee, "An evaluation of the DC-link capacitor heating in adjustable speed drive systems with different utility interface options," in *APEC '99. Fourteenth Annual Applied Power Electronics Conference and Exposition. 1999 Conference Proceedings (Cat. No.99CH36285)*, IEEE, 1999, pp. 781–787 vol. 2, doi: 10.1109/APEC.1999.750457.

[14] S. Peyghami, P. Davari, H. Wang, and F. Blaabjerg, "The impact of topology and mission profile on the reliability of boost-type converters in PV applications," in *2018 IEEE 19th Workshop on Control and Modeling for Power Electronics (COMPEL)*, IEEE, Jun. 2018, pp. 1–8, doi: 10.1109/COMPEL.2018.8460177.

[15] D. Zhou, H. Wang, and F. Blaabjerg, "Mission profile-based system-level reliability analysis of DC/DC converters for a backup power application," *IEEE Transactions on Power Electronics*, vol. 33, no. 9, pp. 8030–8039, 2018, doi: 10.1109/TPEL.2017.2769161.
[16] FIDES Group, "FIDES guide 2009 edition: A reliability methodology for electronic systems." [Online]. Available: https://www.fides-reliability.org
[17] H. Wang and F. Blaabjerg, "Reliability of capacitors for DC-link applications in power electronic converters - An overview," *IEEE Transactions on Industry Applications*, vol. 50, no. 5, pp. 3569–3578, 2014, doi: 10.1109/TIA.2014.2308357.
[18] Y. Song and B. Wang, "Survey on reliability of power electronic systems," *IEEE Transactions on Power Electronics*, vol. 28, no. 1, pp. 591–604, 2013, doi: 10.1109/TPEL.2012.2192503.
[19] G. Perilla Galindo, M. Perez, G. Yamhure, A. Fajardo, and C. I. Paez-Rueda, "Improving circuit and transformer complexity for 24-pulse AC-DC converter topology," *IEEE Access*, vol. 12, pp. 156994–157005, 2024, doi: 10.1109/ACCESS.2024.3480689.
[20] R. Pandurangan, P. Kaliannan, and P. Shanmugam, "Effects of current distortion on DC link inductor and capacitor lifetime in variable frequency drive connected to grid with active harmonic filter," *IEEE Transactions on Industry Applications*, vol. 57, no. 1, pp. 492–505, Jan. 2021, doi: 10.1109/TIA.2020.3028555.
[21] S. Gopalan, K. Vasudevan, D. Kumar, and S. Paramasivam, "Impact of supply voltage unbalance and harmonics on DC bus electrolytic capacitor of adjustable speed drives," *IEEE Transactions on Industry Applications*, pp. 1–1, 2020, doi: 10.1109/TIA.2020.2991133.
[22] Cornell Dubilier Electronics, "CGS screw terminal aluminum electrolytic capacitor catalog (CGS.pdf)." [Online]. Available: https://www.cde.com/resources/catalogs/CGS.pdf
[23] S. Gopalan, S. Mule, D. Kumar, and N. Edlabadkar, "Influence of grid impedance on the DC bus capacitor of an ASD in a multi-drive system," in *2023 IEEE International Conference on Power Electronics, Smart Grid, and Renewable Energy (PESGRE)*, IEEE, Dec. 2023, pp. 1–6, doi: 10.1109/PESGRE58662.2023.10405023.
[24] L. B. K. Fisch, O. H. Gonçalves, F. Trentini, C. A. Hummelgen, and A. J. Rossa, "Impact analysis on variable-speed drives under unbalanced grid conditions," in *2023 IEEE 8th Southern Power Electronics Conference and 17th Brazilian Power Electronics Conference (SPEC/COBEP)*, IEEE, Nov. 2023, pp. 1–8, doi: 10.1109/SPEC56436.2023.10408132.
[25] H. Wang, P. Davari, D. Kumar, F. Zare, and F. Blaabjerg, "The impact of grid unbalances on the reliability of DC-link capacitors in a motor drive," in *2017 IEEE Energy Conversion Congress and Exposition (ECCE)*, IEEE, Oct. 2017, pp. 4345–4350, doi: 10.1109/ECCE.2017.8096748.

BIOGRAPHIES OF AUTHORS

R. Govarthanan received a degree in electrical engineering in the year 2002 from Mepco Schlenk Engineering College, Sivakasi, India, and a master's degree in Power Electronics in the year 2005 from AC College of Engineering and Technology, Karaikudi, India. Currently, he is doing a doctoral program at Vellore Institute of Technology, Vellore, India. He is a part of ESAB R&D-Engineering Services Division, India. His areas of interest include the design of power converters, variable frequency drives, and high frequency magnetics. He can be contacted at email: go4govi@gmail.com.

Dr. K. Palanisamy received the degree in electrical engineering from the KSR College of Technology, Tiruchengode, India, in 2000, the master's (Hos.) degree in applied electronics from the Coimbatore Institute of Technology, Coimbatore, India, in 2004, and the Ph.D. degree in electrical Engineering from the Vellore Institute of Technology, Vellore, India, in 2013. He is currently an associate professor of the energy and power electronics division and the Head of the Centre for Smart Grid Technology, Vellore Institute of Technology, since 2007 to date. From 2016 to 2018, he was the Head of the Department of Energy and Power Electronics Division. He has authored more than 96 scientific papers in refereed conference proceedings and internal journals in the field of renewable energy, battery energy storage, multilevel converters, and power quality. He is a certified Energy Auditor by the Bureau of Energy Efficiency, Government of India. He has taken up various consultancy projects in energy efficiency and power quality improvement. He can be contacted at email: kpalanisamy@vit.ac.in.

Dr. S. Paramasivam received the B.E. degree from the Government College of Technology, Coimbatore, India, in 1995, the M.E degree from the PSG College of Technology, Coimbatore, India, in 1999, and the Ph.D. degree in electrical engineering from the College of Engineering, Anna University, Chennai, India, in 2006. He is presently with ESAB R&D-Engineering Services Division. He has authored or co-authored more than 150 papers on various aspects of SRM and induction motor drives in international journals and conferences worldwide. He has been associated with various international journals in different editorial activities. His research interests include power electronics, ac motor drives, DSP and FPGA-based motor controls, power factor correction, magnetic design, fuzzy logic, neural networks, and controller design for wind energy conversion systems. He can be contacted at email: paramsathya@yahoo.com.